Astronomy & Astrophysics manuscript no. 8892
February 2, 2008

Detection of 'parent' molecules from the inner wind of AGB stars as tracers of non-equilibrium chemistry

L. Decin[1,2⋆], I. Cherchneff[3], S. Hony[4,1], S. Dehaes[1⋆⋆], C. De Breuck[5], and K. M. Menten[6]

[1] Department of Physics and Astronomy, Institute for Astronomy, K.U.Leuven, Celestijnenlaan 200B, B-3001 Leuven, Belgium
e-mail: leen.decin@ster.kuleuven.be
[2] Sterrenkundig Instituut Anton Pannekoek, University of Amsterdam, Kruislaan 403 1098 Amsterdam, The Netherlands
[3] Institut für Astronomie, ETH Hönggerberg, Wolfgang-Pauli-Strasse 16, 8093 Zürich, Switzerland
e-mail: isabelle.chechnneff@phys.ethz.ch
[4] Laboratoire AIM, CEA/DSM - CNRS - Universit Paris Diderot, DAPNIA/SAp, 91191 Gif sur Yvette, France
e-mail: sacha.hony@cea.fr
[5] European Southern Observatory, Karl-Schwarschild Strasse, D-85748 Garching bei München, Germany
e-mail: cdebreuck@eso.org
[6] MPI für Radioastronomie, Auf dem Hügel 69, D-53121 Bonn, Germany
e-mail: kmenten@mpifr-bonn.mpg.de

Received September 15, 2007; accepted October 15, 2007

Abstract

Context. Asymptotic Giant Branch (AGB) stars are typified by strong dust-driven, molecular outflows. For long, it was believed that the molecular setup of the circumstellar envelope of AGB stars is primarily determined by the atmospheric C/O ratio. However, recent observations of molecules such as HCN, SiO, and SO reveal gas-phase abundances higher than predicted by thermodynamic equilibrium (TE) models. UV-photon initiated dissociation in the outer envelope or non-equilibrium formation by the effect of shocks in the inner envelope may be the origin of the anomolous abundances.
Aims. We aim at detecting *(i)* a group of 'parent' molecules (CO, SiO, HCN, CS), predicted by the non-equilibrium study of Cherchneff (2006) to form with almost constant abundances independent of the C/O ratio and the stellar evolutionary stage on the Asymptotic Giant Branch (AGB), and *(ii)* few molecules, such as SiS and SO, which are sensitive to the O- or C-rich nature of the star.
Methods. Several low and high excitation rotational transitions of key molecules are observed at mm and sub-mm wavelengths with JCMT and APEX in four AGB stars: the oxygen-rich Mira WX Psc, the S star W Aql, and the two carbon stars V Cyg and II Lup. A critical density analysis is performed to determine the formation region of the high-excitation molecular lines.
Results. We detect the four 'parent' molecules in all four objects, implying that, indeed, these chemical species form whatever the stage of evolution on the AGB. High-excitation lines of SiS are also detected in three stars with APEX, whereas SO is only detected in the oxygen-rich star WX Psc.
Conclusions. This is the first multi-molecular observational proof that periodically shocked layers above the photosphere of AGB stars show some chemical homogeneity, whatever the photospheric C/O ratio and stage of evolution of the star.

Key words. Astrochemistry, Molecular processes, Stars: AGB and post-AGB, (Stars): circumstellar matter, Stars: mass loss, Submillimeter

1. Introduction

Circumstellar envelopes of Asymptotic Giant Branch stars (AGBs) have long been known to be efficient sites of molecule formation. While the outer layers of such envelopes experience penetration of interstellar UV photons and cosmic rays resulting in a fast ion-molecule chemistry, the deepest layers are dominated by a non-equilibrium chemistry due to the passage of shocks generated by stellar pulsation. Dust forms in those inner gas layers, still bound to the star, and grains couple to the gas to accelerate it, thereby generating stellar wind and mass loss phenomena. The described processes greatly modify the abundances established by the equilibrium chemistry in the dense, hot photosphere (Tsuji 1973).

For a long time, the gas chemical composition was believed to be dominated entirely by the C/O ratio of the photosphere. A C/O ratio greater than one implied that all the oxygen was tied in CO, leading to an oxygen-free chemistry, whereas a C/O ratio less than one meant that no carbon bearing molecules apart from CO could ever form in an oxygen-rich (O-rich) environment. This picture, based essentially on thermal equilibrium considerations applied to the gas, has been first disproved by the detection of SiO at millimeter (mm) wavelength in carbon-rich (C-rich) AGBs (Bujarrabal et al. 1994). As for O-rich AGBs, CO_2 infrared (IR) transition lines were detected in various objects with the Short-Wavelength Spectrometer (SWS) onboard the Infrared Space Observatory (ISO) (e.g., Justtanont et al. 1996; Ryde et al. 1998).

Theoretical modeling describing the chemistry in the inner wind of the extreme carbon star IRC+10216 showed that the formation of SiO was due primarily to hydroxyl OH re-

⋆ *Postdoctoral Fellow of the Fund for Scientific Research, Flanders*
⋆⋆ *Scientific Researcher of the Fund for Scientific Research, Flanders*

action with atomic silicon close to the photosphere as a result of shock activity and therefore non-equilibrium chemistry (Willacy & Cherchneff 1998). Later on, Duari et al. (1999) showed that CO_2 formation in the O-rich Mira IK Tau results from the reaction of OH radicals with CO in the shocked regions, implying again that non-equilibirum chemistry was paramount to the formation of C-bearing species in O-rich Miras. It was then recently proposed that the inner wind of AGBs shows a striking homogeneity in chemical composition, despite their photospheric C/O ratio and stage of stellar evolution (Cherchneff 2006). In particular, Cherchneff (2006) showed that when taking shock chemistry into account, molecules such as SiO, HCN and CS are present in comparable amount in the inner layers of M, S, and C AGBs, whereas specific molecules (e.g. SO and HS for O-rich Miras and C_2H_2 for carbon stars) are typical for O-rich or C-rich chemistries.

In this letter, we present observations carried out with the JCMT and the APEX telescope of four AGBs: one O-rich, WX Psc, one S star ($\equiv$ C/O $\approx$ 1), W Aql, and two carbon stars, II Lup and V Cyg. We focus on the detection of (sub)mm transitions of CO, SiO, HCN, CS, SiS and SO in order to confirm or disprove the above hypothesis and to check for homogeneity in AGB winds.

2. Observations and line profiles

The observations were performed in October 2006 with the 15 m JCMT[1] for V Cyg, WX Psc, and W Aql, and in the period from September till October 2006 with the APEX[2] 12 m telescope for II Lup, WX Psc and W Aql. Due to technical problems with the RxB3 JCMT receiver, only low frequency lines within the RxA3 receiver (211 – 276 GHz) were obtained. For the APEX observations, both the APEX-2A receiver (279–381 GHz) and FLASH receiver (460–495 GHz and 780–887 GHz) were used. The observations were carried out using a position-switching mode. The JCMT data reduction was performed with the SPLAT devoted routines of STARLINK, the APEX-data with CLASS. A polynomial was fitted to an emision free region of the spectral baseline and subtracted. The velocity resolution for the JCMT-data equals to 0.0305 MHz, for the APEX to 0.1221 MHz. For WX Psc, W Aql, and II Lup the data were rebinned to a resolution of 1 km/s, for V Cyg to 0.75 km/s in order to have at least 40 independent resolution elements per line profile. The antenna temperature, T_A^*, was converted to the main-beam temperature ($T_{mb} = T_A^*/\eta_{mb}$), using a main-beam efficiency η_{mb} of 0.69 for the JCMT RxA3 receiver, of 0.73 for the APEX-2A receiver, and of 0.60 and 0.43 for the 460–495 GHz and 780–887 GHz FLASH channels respectively (Güsten et al. 2006).

The observed molecular emission lines of four AGB stars in our sample are displayed in the Figs. 1 – 4.

In all stars molecular emission lines of CO, SiO, HCN, and CS are detected. This confirms the prediction of homogeneity by Cherchneff (2006) as these species being 'parent' molecules which form in the inner layers of the CSE. This can be understood in terms of the chemistry of these four molecules being determined by shock propagation and not by the photospheric C/O ratio and the stellar evolutionary stage.

SiS is also detected in all stars and we were able to detect with APEX the high-excitation SiS(19-18) line in the O-rich WX Psc, the C-rich II Lup and the S-rich W Aql. This is in good agreement with recent SiS OSO, JCMT, and APEX observations of Schöier et al. (2007) in a large sample of M and C stars, including WX Psc and V Cyg. This implies that SiS also forms close to the star, whatever the stage of stellar evolution.

Both the SO(6_5 – 5_4) and the high-excitation SO(10_{11} – 10_{10}) line were detected in O-rich WX Psc. SO was neither found in the S-type W Aql, nor in the two carbon stars II Lup and V Cyg. SO appears to be typical for O-rich AGBs only, supporting the non-detection of SO in C-stars by Woods et al. (2003).

Both optically thin and optically thick lines occur (e.g., ^{13}CO(2-1) versus the ^{12}CO(2-1) line in W Aql, see e.g. Fig. 2). The line parameters, i.e., the main-beam brightness temperature at the line centre (T_{mb}), the line centre velocity (v_*), and half the full line width (v_e), are obtained by fitting the 'soft parabola' line profile function to the data (Olofsson et al. 1993)

$$T(v) = T_{\rm mb}\left[1-\left(\frac{v-v_*}{v_{\rm e}}\right)^2\right]^{\beta/2}, \quad (1)$$

where β describes the shape of the line. The velocity-integrated intensities are obtained by integrating the emission between $v_* \pm v_e$ and are listed in Table 1. A value of $\beta = 2$ represents a parabolic line shape, expected for optically thick expanding spherical envelopes in case the source is much smaller than the radio telescope beam size; $\beta < 0$ results in a profile with horns at the extreme velocity, expected for optically thin lines when the source is resolved (Morris 1975). In our sample, several lines have a β-value distinctly larger than 2, indicating that the line formation occurs partially in the inner region, where the stellar wind has not yet reached its full terminal velocity. This is notably the case for the CS, SiO, and HCN lines in our sample, corroborating their formation close to the star. The estimated terminal velocities for WX Psc, W Aql, II Lup, and V Cyg are 19.2 km/s, 18.8 km/s, 20.1 km/s, and 12.4 km/s, respectively. A maximum of 5 % difference is found in the derived terminal velocity values for each target, being within the velocity binsize, indicating that all of the detected lines at least partly survive the dust formation and wind acceleration processes. An exception is SiS(19-18) in WX Psc (16 km/s), but particularly the SO(10_{11}-10_{10}), with an estimated terminal velocity of only 10 km/s, traces a much smaller geometrical region.

3. Excitation analysis

In case many transitions of an individual molecule can be observed, it is possible to assess whether collisional or radiative excitation mechanisms can produce the observed line intensities. While it is well known that CO is formed in both M, C and S-type stars and survives dust condensation, it is of interest to study the excitation requirements for the three other 'parent' molecules SiO, HCN and CS predicted by Cherchneff (2006) to be abundant in the inner winds of M, S and C AGBs.

For all lines, except for those from the CO molecule, the emission distribution is expected to be much smaller than the FWHM beam size of the used telescope. To calculate column densities we need to correct for the different beam filling factor, $f = \theta_S^2/(\theta_S^2+\theta_B^2)$, with θ_B and θ_S being the FWHM of the beam and the source respectively. To do this, we define a beam-averaged brightness temperature, T_b, scaled by correcting our

[1] The James Clerk Maxwell Telescope (JCMT) is operated by The Joint Astronomy Centre on behalf of the Science and Technology Facilities Council of the United Kingdom, the Netherlands Organisation for Scientific Research, and the National Research Council of Canada. Program ID is m06bn03 (34 h).

[2] APEX, the Atacama Pathfinder Experiment, is a collaboration between the Max-Planck-Institut fur Radioastronomie, the European Southern Observatory, and the Onsala Space Observatory. Program ID is ESO.078.D-0534 (44 h).

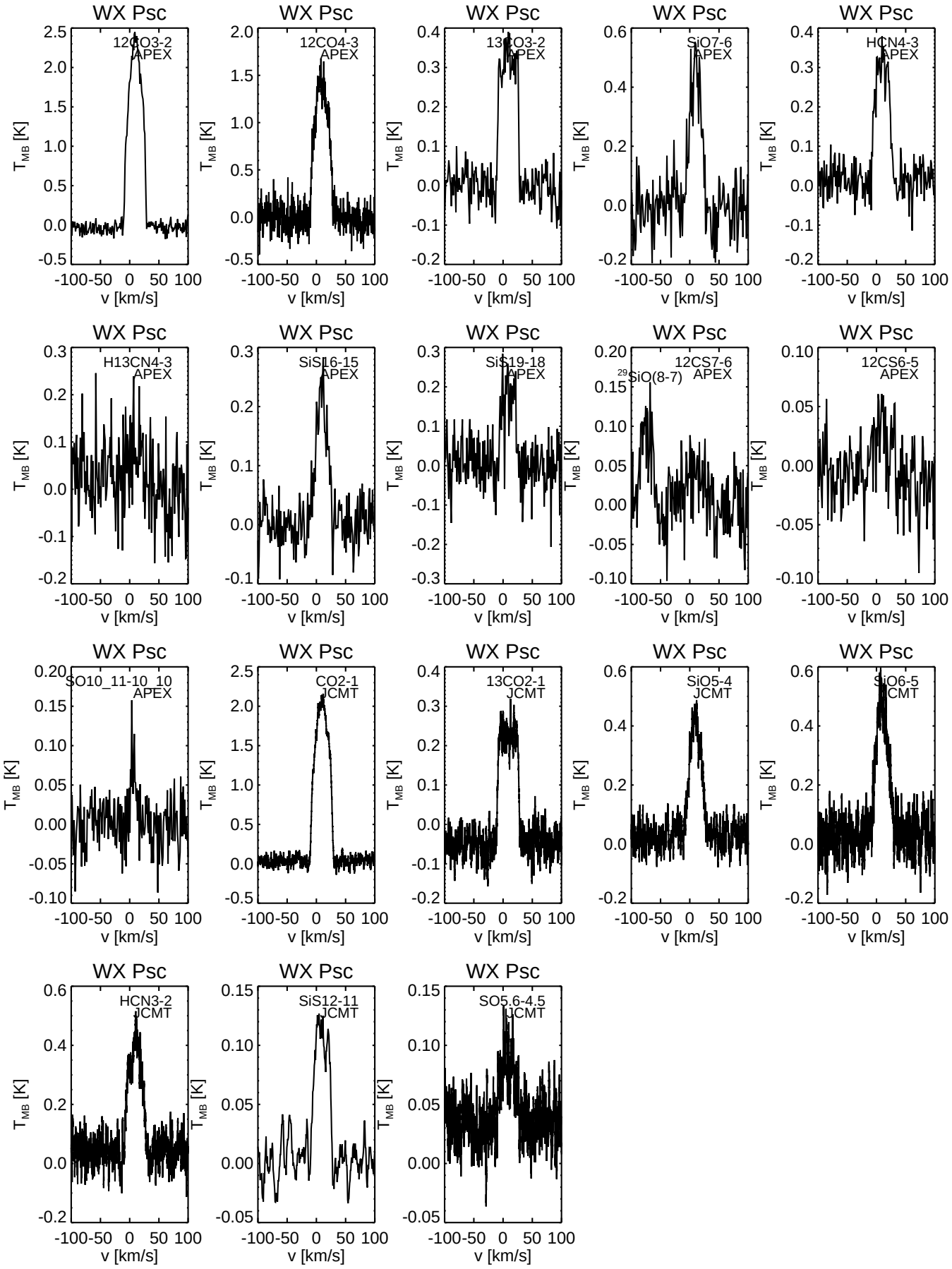

Figure 1. Molecular emission detected with APEX and JCMT in the O-rich AGB WX Psc.

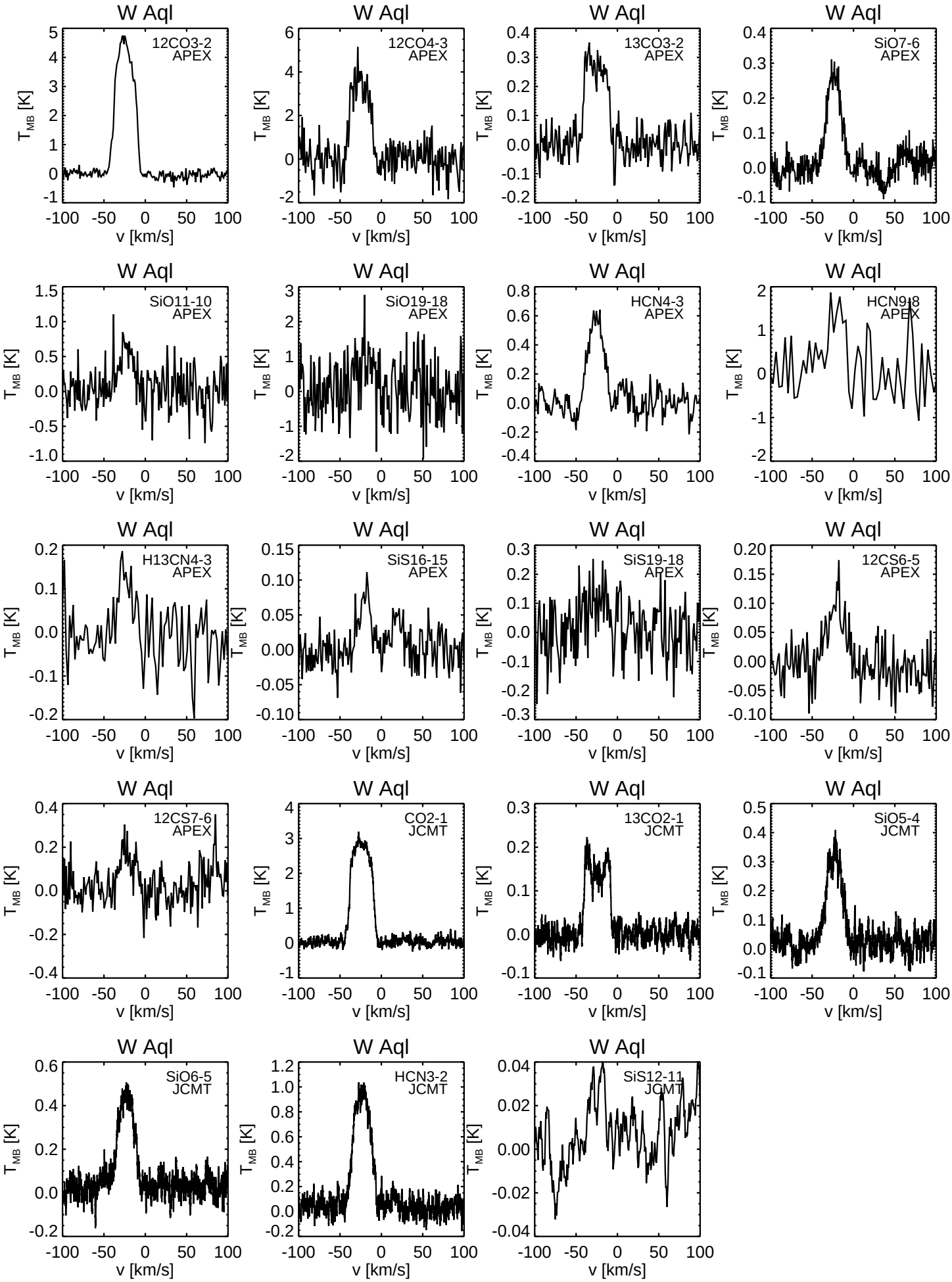
W Aql
12CO3-2 APEX
12CO4-3 APEX
13CO3-2 APEX
SiO7-6 APEX
SiO11-10 APEX
SiO19-18 APEX
HCN4-3 APEX
HCN9-8 APEX
H13CN4-3 APEX
SiS16-15 APEX
SiS19-18 APEX
12CS6-5 APEX
12CS7-6 APEX
CO2-1 JCMT
13CO2-1 JCMT
SiO5-4 JCMT
SiO6-5 JCMT
HCN3-2 JCMT
SiS12-11 JCMT
T_MB [K]
v [km/s]

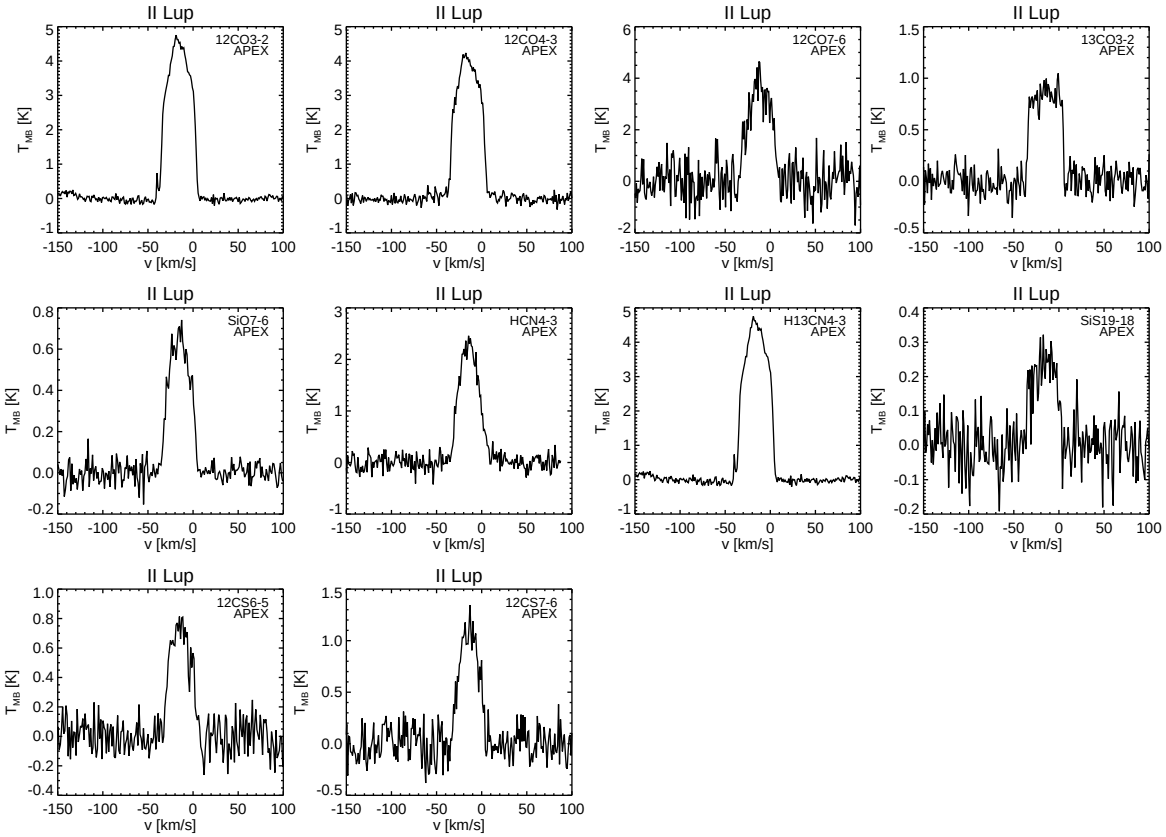

Figure 3. Molecular emission detected with APEX in the C-rich AGB II Lup.

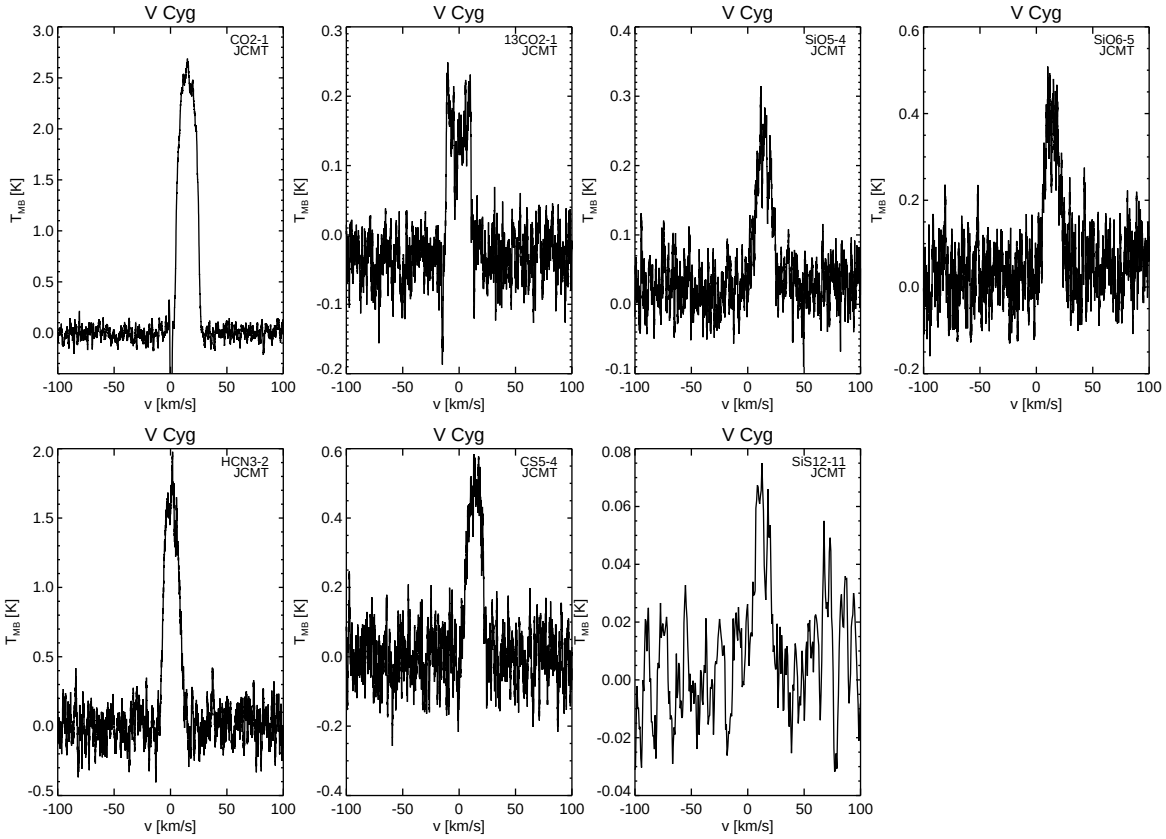

Figure 4. Molecular emission detected with JCMT in the C-rich AGB V Cyg.

Table 1. Overview of the velocity-integrated intensities ($\int T_{mb}\,dv$ in K km/s) for the observed line transitions. The frequency is listed in GHz and the lower energy level in cm^{-1}. The integrated intensity of detected lines with a low S/N-ratio is given between brackets. In case of a non-detection, an upper limit on the integrated intensity is computed as $3\sigma\times$ expected linewidth, with σ the noise on the data. A '$-$' indicates lines that were not observed. APEX-data are reported upright, JCMT-data are given in italics.

transition	*^{12}CO(2-1)*	^{12}CO(3-2)	^{12}CO(4-3)	^{12}CO(7-6)	*^{13}CO(2-1)*	^{13}CO(3-2)	*^{12}CS(5-4)*	^{12}CS(6-5)	^{12}CS(7-6)	^{12}CS(10-9)	^{12}CS(17-16)
frequency	*230.538*	345.795	461.040	806.651	*220.398*	330.587	*244.935*	293.912	342.882	489.759	832.061
$E_{\rm low}$	*3.84*	11.54	23.07	80.74	*3.67*	11.03	*16.34*	24.51	34.32	75.53	222.15
WX Psc	*58.0*	64.3	40.2	22.4	*9.9*	11.3	*<2.4*	[0.8]	1.3	<8.1	<42.6
W Aql	*80.6*	118.4	95.9	<178	*4.6*	8.1	–	2.4	4.6	<54.1	<203
II Lup	–	145.0	130.0	99.7	–	32.5	–	20.4	35.2	–	–
V Cyg	*45.6*	–	–	–	*4.2*	–	*7.4*	–	–	–	–

transition	^{13}CS(7-6)	^{13}CS(10-9)	*H^{12}CN(3-2)*	H^{12}CN(4-3)	H^{12}CN(9-8)	H^{13}CN(4-3)	*SiO(5-4)*	*SiO(6-5)*	SiO(7-6)	SiO(11-10)
frequency	323.684	462.334	*265.886*	354.505	797.433	345.340	*217.105*	*260.518*	303.926	477.504
$E_{\rm low}$	32.39	69.41	*8.87*	17.74	106.42	17.28	*14.48*	*21.73*	30.42	79.65
WX Psc	<67.4	<12.7	*9.9*	8.9	<117	[2.6]	*9.2*	*11.1*	10.4	<15.0
W Aql	–	<13.0	*21.7*	12.2	[34.1]	3.1	*7.1*	*8.9*	5.2	13.8
II Lup	–	–	–	60.7	–	64.2	–	–	19.6	–
V Cyg	–	–	*25.7*	–	–	–	*3.8*	*5.1*	–	–

transition	SiO(19-18)	SiS(12-11)	*SiS(14-13)*	SiS(16-15)	SiS(19-18)	SO(1_1-1_0)	*SO(6_5-5_4)*	SO(7_8-6_7)	*SO(8_9-8_8)*	SO(10_{11}-10_{10})
frequency	824.235	217.817	*254.102*	290.380	344.778	286.34	*219.949*	340.714	*254.573*	336.597
$E_{\rm low}$	247.57	39.96	*55.10*	72.66	103.53	1.00	*16.98*	45.10	*60.80*	88.08
WX Psc	<92.2	*3.2*	*<1.2*	5.4	4.8	<0.9	*1.6*	<1.4	<2.0	[0.9]
W Aql	[22.3]	–	–	1.2	[3.4]	–	*<1.2*	<3.4	–	–
II Lup	–	–	–	–	7.8	–	–	<4.2	–	–
V Cyg	–	*0.9*	*<14.8*	–	–	–	*<1.3*	–	–	–

main-beam brightness temperatures for a fictitious $10''$ FWHM source, i.e, $T_b = 1/f \times T_{mb}$.

Little interferometric data exist for the molecules that we have observed in *any* circumstellar envelope. We note, however, that $4''$–$6''$ resolution observations of the HCN $J = 1-0$ line in the Mira variables TX Cam and IK Tau (Marvel 2005) barely resolve the emission distibutions in these objects. Since, first, those objects are closer to the Sun than our target stars and, second, our higher exciation lines most likely arise from more compact regions than the $1-0$ line, the column densities derived are strict lower limits.

Assuming that the lines are optically thin and that the excitation temperature, T_{ex}, between upper and lower level is such that $T_{ex} \gg T_{bg}$ (with T_{bg} the temperature of any background source, e.g. 2.7 K), the integration of the standard radiative transfer equation shows that (Goldsmith & Langer 1999)

$$N_u = \frac{1.67\times10^{14}}{\nu\ \mu^2}\left(\int T_b\,dv\right)\,, \tag{2}$$

with N_u the column density of the upper transition state in cm^{-2}, μ the transition dipole moment in Debye, ν the transition frequency in GHz, T_{mb} the main-beam temperature in Kelvin and v the velocity in km/s. For rotational transitions, the transition moment for diatomic and polyatomic molecule is given by

$$\mu^2(J+1,J) = \frac{J+1}{2J+3}\,\mu_e^2\,, \tag{3}$$

where μ_e is the permanent dipole moment of the molecule. Using the velocity–integrated intensities of Table 1, we calculate the resulting upper state column densities (see Table 2).

Assuming purely collisional excitation, and ignoring radiation trapping, one can derive from solving the statistical equilibrium equation that (Tielens 2005)

$$\frac{N_l}{N_u} = \frac{g_l}{g_u}\left(\frac{n_{\rm crit}}{n_{\rm H_2}}+1\right)\exp(h\nu/kT_{\rm kin})\,, \tag{4}$$

where N_u, N_l, g_u, g_l are the upper and lower state column densities and degeneracies, $T_{\rm kin}$ the kinetic temperature, $n_{\rm crit}$ the critical density, and $n_{\rm H_2}$ the hydrogen density. For a multi-level system, the critical density is given by (Tielens 2005)

$$n_{\rm crit} = \frac{\sum_{l<u} A_{ul}}{\sum_{l\neq u}\gamma_{ul}}\,, \tag{5}$$

where A_{ul} represents the Einstein coefficient, and γ_{ul} the collisional rate coefficients. Critical densities were calculated at differing temperatures using the data available in the LAMDA-database (Schöier et al. 2005) (see Table 2). Applying Eq. (4) together with the column densities from Table 2, the minimum density requirements for $n_{\rm H_2}$ to achieve the observed number-density ratios are tabulated in Table 3. Note that the listed values are at $T_{\rm kin} = 300$ K, and that for lower temperatures the critical density increases.

The gas temperature, density and velocity structure was calculated in a self-consistent way using the GASTRoNOoM-code (Decin et al. 2006) to determine where in the envelope the gas density falls below the density requirements given in Table 3 (see Fig. 5). The assumed stellar parameters are listed in Table 4, and the derived (maximum) radius of the emitting region is listed in Table 3. If collisional excitation is assumed, it appears from Table 3 that the 'parent' molecules SiO, HCN and CS are excited in the inner ($\lesssim 20\,{\rm R}_*$) and intermediate ($\lesssim 70\,{\rm R}_*$) regions of the circumstellar envelope and trace regions after the dust condensation zone where they have been injected from deeper layers.

It is also of interest to consider the case where collisional excitation is ignored, and the molecules are excited by infrared radiation from the star. One can derive that (Tielens 2005)

$$\frac{N_l}{N_u} = \frac{g_l}{g_u}\frac{\exp(h\nu/kT_*)-1}{W}+1\,, \tag{6}$$

where W is the geometrical dilution, being $(R_*/2R)^2$ when R$\gg$R$_*$. As seen from Table 3, radiative excitation constrains the emitting zone for SiO being $\lesssim$9 R$_*$, for HCN $\lesssim$ 13 R$_*$, and for

Table 2. Velocity-integrated intensities (in K km/s), upper state column densities in cm^{-2} calculated using Eq. (2) and critical densites in cm^{-3} for the detected multiple-transitions 'parent' molecules used in the excitation analysis. In a few cases, extra integrated-intensity values (listed in italics) as found in literature are added to perform the excitation analysis. Literature references are given in the footnote.

		SiO (5-4)	SiO (6-5)	SiO (7-6)	SiO (8-7)	HCN(3-2)	HCN(4-3)	CS(5-4)	CS(6-5)	CS(7-6)
WX Psc	$\int T_{mb}\,dv$	9.2	11.1	10.4		9.9	8.9	2.4	[0.8]†	1.3
	N_u	7.96×10^{12}	7.91×10^{12}	5.15×10^{12}		7.96×10^{12}	4.22×10^{12}	2.53×10^{12}	1.08×10^{12}	1.41×10^{12}
W Aql	$\int T_{mb}\,dv$	7.1	8.9	5.2		21.7	12.2	*8.5*[a]	2.3	4.6
	N_u	6.19×10^{12}	6.36×10^{12}	2.57×10^{12}		1.74×10^{13}	5.81×10^{12}	8.95×10^{12}	3.03×10^{12}	5.00×10^{12}
II Lup	$\int T_{mb}\,dv$			19.62	*20.4*[b]	*139.76*[c]	60.69	*32.34*[c]	20.37	35.24
	N_u			6.96×10^{12}	8.74×10^{12}	1.24×10^{14}	2.88×10^{13}	6.85×10^{13}	2.61×10^{13}	3.83×10^{13}
V Cyg	$\int T_{mb}\,dv$	3.8	5.1		*8.4*[d]	25.7	*31.9*[d]	7.4		
	N_u	3.33×10^{12}	3.51×10^{12}		5.28×10^{12}	2.06×10^{13}	1.51×10^{13}	1.41×10^{13}		
at 40 K	$n_{\rm crit}$	3.06×10^6	5.26×10^6	8.41×10^6	1.27×10^7	5.83×10^6	1.32×10^7	1.85×10^6	3.22×10^6	5.09×10^6
at 100 K	$n_{\rm crit}$	2.00×10^6	3.44×10^6	5.57×10^6	8.18×10^6	4.22×10^6	9.63×10^6	1.35×10^6	2.37×10^6	3.76×10^6
at 300 K	$n_{\rm crit}$	1.22×10^6	2.10×10^6	3.44×10^6	5.12×10^6	2.35×10^6	5.65×10^6	8.35×10^5	1.48×10^6	2.37×10^6

[a] Bujarrabal et al. (1994); [b] Schöier et al. (2006); [c] Woods et al. (2003); [d] Bieging et al. (2000)
† line detected however with small S/N so that the integrated intensity is quite uncertain

Table 3. For each target, the first row lists the minimum number density for $n_{\rm H_2}$ in cm^{-3} as derived using Eq. (4) at $T_{\rm kin} = 300$ K and the second row gives the corresponding maximum radius for the emission regions obtained using the GASTRoNOoM-code. The third row gives the maximum radius for the emitting region calculated using Eq. (6).

		SiO	HCN	CS
WX Psc	$n_{\rm H_2}$	5.0×10^6	4.4×10^6	9.0×10^5
	R [Eq. (4)]	17 R_*	19 R_*	33 R_*
	R [Eq. (6)]	4.5 R_*	6 R_*	7.5 R_*
W Aql	$n_{\rm H_2}$	2.1×10^6	2.1×10^6	6.34×10^5
	R [Eq. (4)]	40 R_*	40 R_*	70 R_*
	R [Eq. (6)]	9 R_*	10 R_*	11 R_*
II Lup	$n_{\rm H_2}$	2.7×10^7	1.3×10^6	7.6×10^5
	R [Eq. (4)]	13 R_*	53 R_*	70 R_*
	R [Eq. (6)]	2.5 R_*	13 R_*	10 R_*
V Cyg	$n_{\rm H_2}$	2.8×10^7	8.7×10^6	
	R [Eq. (4)]	5 R_*	9 R_*	
	R [Eq. (6)]		4 R_*	

Table 4. Stellar parameters used as input for the GASTRoNOoM-code. The terminal velocity, v_∞, is derived from the CO lines; the stellar radius from the stellar luminosity and temperature. The envelope density falls off as $\sim r^{-2}$. Literature references are given in the footnote.

	WX Psc	W Aql	II Lup	V Cyg
T_* [K]	2000[a]	2800	2400[f]	1900[f]
R_* [10^{13} cm]	5.5	2.4	3.8	5.1
L_* [10^3 $L_\odot$]	10[a]	6.8[b]	8.8[f]	6.3[f]
[CO]/[H_2] [10^{-4}]	3[c]	6[c]	8[c]	8[c]
distance [pc]	833[a]	230[d]	500[f]	310[f]
$R_{\rm inner}$ [R_*]	5[a]	8[e]	4[f]	2[f]
v_∞ [km/s]	18	17.5	21	10.5
$\dot{M}$ [10^{-6} $M_\odot$ yr^{-1}]	6[a,†]	2.5[b]	9[f]	1.2[g]

[a] Decin et al. (2007); [b] Ramstedt et al. (2006); [c] Knapp & Morris (1985); [d] Bieging et al. (2000); [e] Danchi et al. (1994); [f] Schöier et al. (2006); [g] Schöier & Olofsson (2001)
[†] refers to the inner region (A) in Decin et al. (2007)

CS $\lesssim$11 R_*. In general, these regions are smaller than derived in case of collisional excitation, indicating that the radiation field of the star does not have enough energy to sustain the excitation. An analogous expression as for Eq. (6) can be derived for a radiation field characterized by a dust temperature T_d at the condensation radius $R_{\rm inner}$, with the dilution factor then being $(R_{\rm inner}/2R)^2$. Using the dust condensation radii listed in Table 4 and a dust temperature of 800 K the derived emitting regions are a factor 3.2 larger for WX Psc, a factor 4.3 for W Aql, a factor 4 for II Lup, and a factor 2 for V Cyg, resulting in similar radii as in case of collisional excitation.

Although the numbers in Table 3 can only be used as rough guidelines, they suggest in both cases a sequence in the excitation pattern, SiO being the species emitting the closest to the star, followed by HCN and CS.

4. Conclusions

From the above analysis, one can draw the following conclusions:

1. The observations reported in this letter confirm the status of 'parent' molecules for CO, SiO, HCN, and CS in AGB stars, whose observed molecular lines form close to the star in support of the theoretical predictions of Cherchneff (2006). The excitation analysis suggests that SiO is emitted closest to the star, followed by HCN and CS.
2. High-excitation lines of SiS are detected in all stars, implying that SiS too forms close to the star, whatever the stage of stellar evolution. However, a thorough line analysis is necessary to prove or disprove that SiS is more abundant in C stars than in O-rich Miras, as predicted by Cherchneff (2006).
3. SO appears to be typical of O-rich AGBs only. With only two excitation lines detected, no information can be drawn on the locus of SO formation. However, the SO(10_{11}-10_{10}) line has an estimated velocity of only 10 km/s in WX Psc when the wind terminal velocity for this object is 19.2 km/s. This fact suggests that the line excitation occurs close to star. In any case, the inner chemistry of O-rich AGB envelopes appears to be as rich, if not richer, than that of C-rich stars.

A detailed line analysis of the present data coupled to further observational campaigns with JCMT and APEX are planned to corroborate these results.

Acknowledgements. LD and SD acknowledge financial support from the Fund for Scientific Research - Flanders (Belgium), IC acknowledges support from the Swiss National Funds for Science through a Marie-Heim-Vögtlin Fellowship,

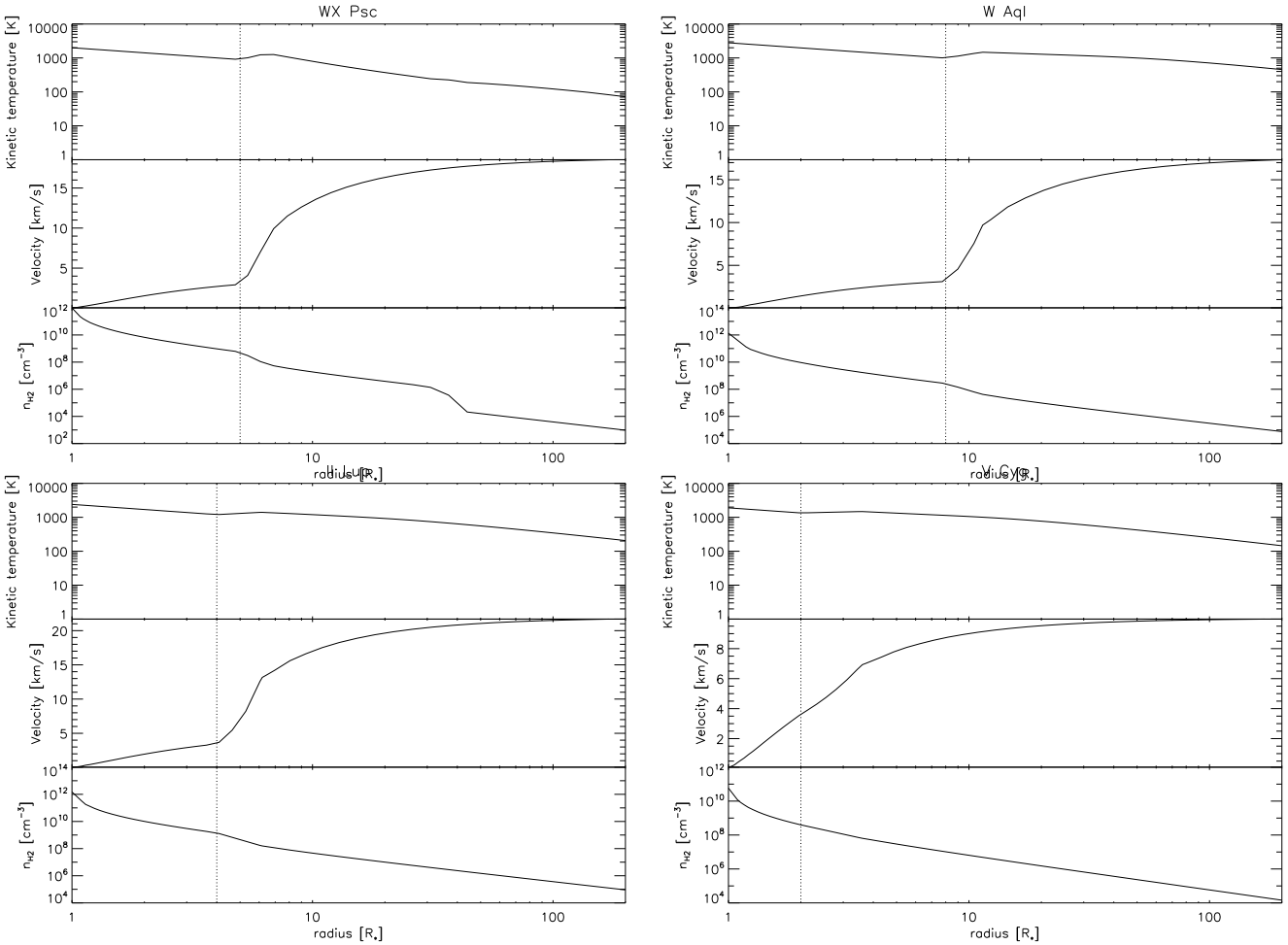

Figure 5. The structure of the CSE as derived using the GASTRoNOoM-code is shown for the four studied targets WX Psc, W Aql, II Lup, and V Cyg. Since the focus is on the inner and intermediate regions, only the first 200 $R_\star$ are displayed. *Upper panel:* Estimated temperature profile, *middle panel:* estimated gas velocity structure, and *bottom panel:* estimated hydrogen density $n_{\rm H_2}$. The dashed line indicates the dust condensation radius, $R_{\rm inner}$. The variable mass-loss rate of WX Psc, mostly noticeable in the hydrogen density, is discussed in Decin et al. (2007).

and SH acknowledges financial support from the Interuniversity Attraction Pole of the Belgian Federal Science Policy P5/36. We thank Remo Tilanus (JCMT) for his support during the observations and reduction of the data.

References

Bieging, J. H., Shaked, S., & Gensheimer, P. D. 2000, ApJ, 543, 897
Bujarrabal, V., Fuente, A., & Omont, A. 1994, A&A, 285, 247
Cherchneff, I. 2006, A&A, 456, 1001
Danchi, W. C., Bester, M., Degiacomi, C. G., Greenhill, L. J., & Townes, C. H. 1994, AJ, 107, 1469
Decin, L., Hony, S., de Koter, A., et al. 2006, A&A, 456, 549
—. 2007, A&A, 475, 233
Duari, D., Cherchneff, I., & Willacy, K. 1999, A&A, 341, L47
Goldsmith, P. F. & Langer, W. D. 1999, ApJ, 517, 209
Güsten, R., Nyman, L. Å., Schilke, P., et al. 2006, A&A, 454, L13
Justtanont, K., de Jong, T., Helmich, F. P., et al. 1996, A&A, 315, L217
Knapp, G. R. & Morris, M. 1985, ApJ, 292, 640
Marvel, K. B. 2005, AJ, 130, 261
Morris, M. 1975, ApJ, 197, 603
Olofsson, H., Eriksson, K., Gustafsson, B., & Carlstrom, U. 1993, ApJS, 87, 267
Ramstedt, S., Schöier, F. L., Olofsson, H., & Lundgren, A. A. 2006, A&A, 454, L103
Ryde, N., Eriksson, K., Gustafsson, B., Lindqvist, M., & Olofsson, H. 1998, Ap&SS, 255, 301
Schöier, F. L., Bast, J., Olofsson, H., & Lindqvist, M. 2007, A&A, *(in press)*
Schöier, F. L., Fong, D., Olofsson, H., Zhang, Q., & Patel, N. 2006, ApJ, 649, 965
Schöier, F. L. & Olofsson, H. 2001, A&A, 368, 969
Schöier, F. L., van der Tak, F. F. S., van Dishoeck, E. F., & Black, J. H. 2005, A&A, 432, 369
Tielens, A. G. G. M. 2005, The Physics and Chemistry of the Interstellar Medium (Cambridge University Press)
Tsuji, T. 1973, A&A, 23, 411
Willacy, K. & Cherchneff, I. 1998, A&A, 330, 676
Woods, P. M., Schöier, F. L., Nyman, L.-Å., & Olofsson, H. 2003, A&A, 402, 617